doi: 10.15407/ujpe62.05.0382

V.Z. KOCHMARSKII,[1] V.R. GAYEVSKII,[1] N.L. TYSHKO[2]

[1] National University of Water Management and Nature Resources Use
(11, Soborna Str., Rivne 33028, Ukraine; e-mail: v.z.kochmarskii@nuwm.edu.ua)
[2] Ivan Franko National University of Lviv
(8, Kyrylo i Mefodiy Str., Lviv 79005, Ukraine)

CALCIUM CARBONATE CRYSTALLIZATION FROM HYDROCARBONATE SOLUTIONS

PACS 82.20Nk, 82.20Ln

The kinetics of $CaCO_3$ precipitation from model solutions formed by preliminary saturating deionized water with CO_2 and by adding $NaHCO_3$ and $CaCl_2$ has been considered. The characteristic feature of the method is the almost simultaneous measurement of the activities of major components of the aqueuos calcium hydrocarbonate system (ACHCS): Ca^{2+}, CO_2, HCO_3^-, as well as pH and the temperature. $CaCO_3$ crystallization was provided with the help of the CO_2 degassing by air. The processes running in the ACHCS during the degassing can be divided into four stages: dissociation of $CaHCO_3^+$ complexes; formation of crystal nuclei in the solution; a transitive stage, which includes the final phase of crystal nucleation and the initial growth of newly formed crystals; and intensive growth of crystal nuclei, which gives rise to the mass $CaCO_3$ precipitation. The product $(Ca^{2+})\cdot(CO_3^{2-})$ is a reaction coordinate for the second stage of $CaCO_3$ precipitation, whereas $(Ca^{2+})\cdot(HCO_3^-)$ for the third and fourth stages. The kinetics of growth of crystal nuclei and their concentration are calculated for the second stage, by using the concept of $CaCO_3$ dissolution product that depends on the crystal nucleus size. During the process of crystal nucleation, the crystal size remains practically stable ($\approx 8\times 10^{-8}$ m), and the concentration reaches 1.5×10^{-15} m^{-3}. The mass $CaCO_3$ precipitation (the fourth stage) starts when the crystal nuclei reach dimensions of about 3×10^{-7} m.

Keywords: calcium carbonate crystallization, reaction coordinate, crystal nuclei, $CaCO_3$ precipitation stages.

1. Introduction

The study of the process of calcium carbonate crystallization is very important in order to understand the circulation of carbon dioxide in nature, in particular, its accumulation in ocean bottom deposits, as well as many technological processes running in water that circulates in cooling systems used in power industry, chemical technologies, and oil and gas mining. However, for now, there is no common viewpoint concerning the kinetics of crystalline $CaCO_3$ extraction from hydrocarbonate solutions, as well as the understanding that different stages of this process are described by different kinetic equations that reflect the mechanisms of crystalline $CaCO_3$ extraction at each stage.

Therefore, this work is devoted to the experimental study of and the formulation of kinetic equations for various stages of extracting crystallite $CaCO_3$. In particular, we are interested in the initial stage associated with the $CaCO_3$ nucleation under controllable conditions and the final stage, which is governed by the diffusion mechanism of material transport to the nuclei.

2. Experimental Part

Researches were carried out on an installation AKVA-2M [1, 2]. A chemically pure $NaHCO_3$ solution prepared with the use of deionized water with a conductivity of 0.2–0.3 mS/m was pourred into a temperature-stabilized measuring cell with double walls. The cell was fabricated from Pyrex glass and had a volume of 50 ml. The temperature $t = (25 \pm 0.1)$ °C was stabilized stage-by-stage. Then the parameters of the initial state were fixed with the help of ion-selective electrodes (calcium electrode ELIS-121Ca, pH electrode ESL-63-07, and reference electrode EBL-1M3) with a discreteness of 27 s (measurements

$i = 1 \div 20$). Afterward, the solution was saturated with chemically pure CO_2 (the data $i = 21 \div 45$). Simultaneously with the CO_2 saturation, 5×50 μl of chemically pure $CaCl_2$ solution with a concentration of 1 M were dosed into the cell. As a result, a $CaCl_2$ concentration of 5.0 mM at an initial $NaHCO_3$ concentration of 10.0 mM in the cell was obtained.

After each dosing, a pause of 1–2 min was maintained in order to establish the electrode potential of ion-selective sensors, and the data on the Ca^{2+} concentration were registered with the help of a computer. The data were used to calculatethe calibration parameters of the calcium electrode with the use of a computer code (the calibration correlation was not worse that 0.999). The monitoring over CO_2 was provided, by using a gas-selective electrode of the Radelkis firm.

The preparation stage corresponds to the measurements $i < 50$ and is not shown in Fig. 1. From the measurement $i = 51$, the degassing of the solution with a constant temperature from CO_2 by air was started. The air was blown through a porous metal sprayer. The degassing intensity was controlled, by using a gas rotameter in the automatic regime by simultaneously inquiring a series of six sensors with a period of 27 s ($i = 51 \div 301$). In the series, the interval between the measurements was about 1 s. The following parameters were measured: time (s), t (°C), pH, pCO_2, pCa, and pCO_3. The removal of CO_2 from the solution initiated the precipitation of crystalline $CaCO_3$.

3. Results and Their Discussion

In Figs. 1–6, the results of researches dealing with the extraction of crystallite $CaCO_3$ are shown for a series of five measurements.

In Fig. 1, a thick curve corresponds to the activity of Ca^{2+} ions averaged over five measurements. One can see that the dispersion is appreciable at the final stage of extraction of the crystallite phase and does not exceed 7–8%.

The kinetic curve for calcium includes a characteristic section corresponding to measurements $i = 50 \div 70$ (540 s in duration), where the growth of the active concentration of Ca^{2+} ions is registered. This growth can be explained by the decay of $CaHCO_3^+$ and $CaCO_3^0$ complexes initiated by the CO_2 degassing from the parent solution according to the reactions

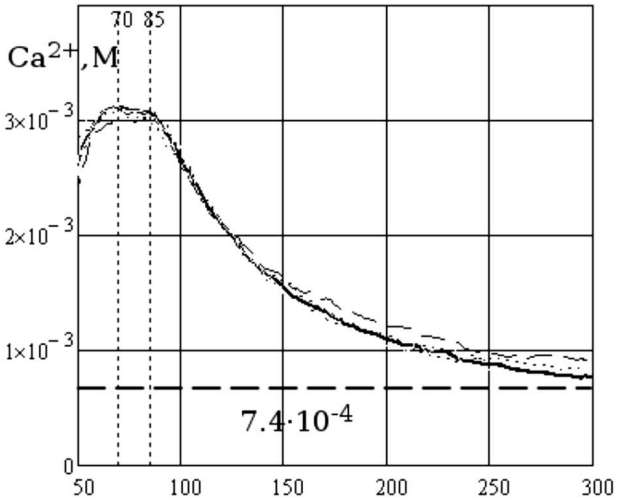

Fig. 1. Kinetics of the Ca^{2+} ion activity in a reaction cell. Degassing and data registration are executed from the measurement $i = 51$. A characteristic feature in the behavior of the Ca^{2+} activity is its growth before the measurement $i = 70$ followed by a recession, which is accelerated at $i > 85$ and is induced by the formation and growth of crystaline nuclei. $\Delta i = 27$ s

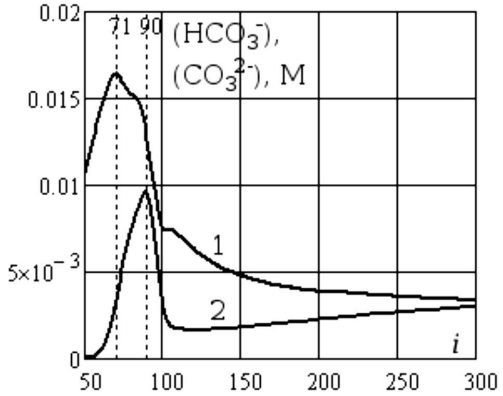

Fig. 2. Kinetic curves for the HCO_3^- (*1*) and CO_3^{2-} (*2*) activities in the CO_2 degassing regime. $\Delta i = 27$ s. Curve *1* was calculated by solving the corresponding kinetic equation. The experimental CO_3^{2-} activity is scaled up by a factor of 50

$$CaHCO_3^+ \rightarrow Ca^{2+} + CO_2 \uparrow + OH^-; \quad (1a)$$

$$CaCO_3^0 + HOH \rightarrow Ca^{2+} + HCO_3^- + OH^-; \quad (1b)$$

$$HCO_3^- \rightarrow CO_2 \uparrow + OH^-; \quad (1c)$$

$$HCO_3^- + OH^- \rightarrow CO_3^{2-} + HOH. \quad (1d)$$

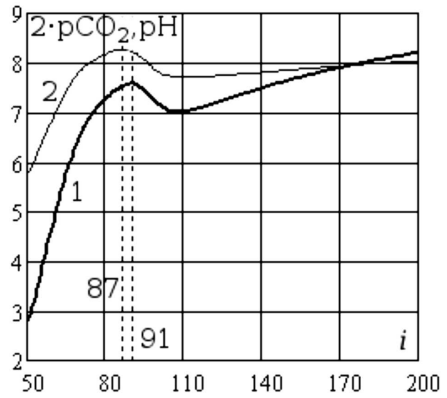

Fig. 3. Kinetics of pCO_2 (*1*) and pH (*2*) during the degassing of ACHCS. Pay attention that pH decreases earlier than pCO_2 by $\Delta i = 4$ (108 s)

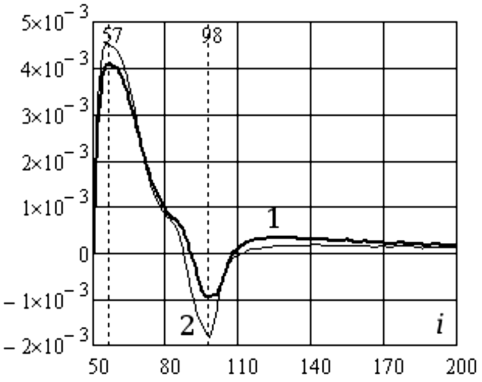

Fig. 4. Kinetics of the derivatives $\Delta pCO_2/\Delta t$ and $\Delta pH/\Delta t$ during the "degassing". The maximum rate of internal generation of CO_2 and hydrogen ions, which is associated with the precipitation of crystalline $CaCO_3$, occurs at $i > 90$

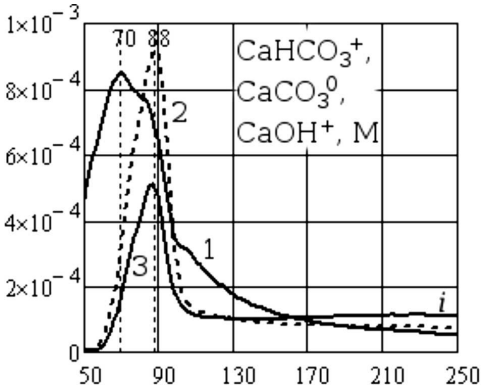

Fig. 5. Kinetic curves for $CaHCO_3^+$ (*1*), $CaCO_3^0$ (*2*), and $CaOH^+$ (*3*) complexes. The $CaOH^+$ concentration is scaled up by a factor of 3000

Note that reaction (1d) is the slowest, because it is associated with the interaction between similarly charged ions.

The behavior of the HCO_3^- and CO_3^{2-} activities is shown in Fig. 2 by curves *1* and *2*, respectively. One can see that, in the interval $i = 51 \div 71$, the active concentration of HCO_3^- grows, which results from the hydrolysis of dissolved CO_2 and the decay of $CaHCO_3^+$ complexes. However, later, at $i > 71$, the HCO_3^- decreases owing to the removal of CO_2 and the precipitation of crystallite $CaCO_3$ (curve *2*). It is of interest that the activity of HCO_3^- ions (curve *1*) has a sharp maximum at $i = 71$, whereas the activity of CO_3^{2-} ions (curve *2* at $i = 90$ (pH = 8.28). This time interval $\Delta t = 513$ s may probably correspond to the time of reaction (1d) under these conditions.

The recession in the CO_3^{2-} activity can also be connected with the intense formation of the crystallite $CaHCO_3^+$ phase and the accompanying release of H^+ and CO_2, which acidify the solution (see Figs. 3 and 4 and Eq. (2)). The slow growth of the CO_3^{2-} activity at $i > 116$ is associated with the pH growth in the aqueous calcium-hydrocarbonate system owing to the removal of CO_2 (see Fig. 3).

The dynamics of pH and pCO_2 are shown in Fig. 3. From those figures, it follows that, starting from $i = 57$ (Fig. 4), the rates of pH and pCO_2 growth drastically decrease. This fact can be explained by the formation of the crystallite phase of calcium carbonate following the scheme

$$\begin{aligned} &Ca^{2+} + 2HCO_3^- \rightarrow CaCO_3 \downarrow + H^+ + HCO_3^-; \\ &H^+ + HCO_3^- \rightarrow CO_2 \uparrow + H_2O. \end{aligned} \qquad (2)$$

This process is accompanied by the generation of H^+ ions and the release of CO_2. From Fig. 3, one can see that the generation of H^+ ions advances the generation of CO_2 by 108 s, which confirms, in general, the sequence of reactions (2) and corresponds to the characteristic time of CO_2 hydrolysis [3].

From Fig. 4, it follows that, concerning the nucleation of the crystalline $CaCO_3$ phase, the most interesting is the measurement interval $57 < i < 98$, where the behaviors of pCO_2 and pH undergo characteristic modifications. Hence, the interval $i = 57 \div 98$ can be regarded as a section, where the $CaCO_3$ crystals are nucleated.

The kinetics of ionic calcium complexes is shown in Fig. 5. Here, curve *1* corresponds to the $CaHCO_3^+$

complex, curve *2* to $CaCO^0$, and curve *3* to $CaOH^+$. The maximum concentration of the calcium bicarbonate complex is about 0.84 mM, and that of the calcium carbonate one about 0.9 mM. Note that the concentration of the calcium hydrate complex is three orders of magnitude lower, and it does not affect processes in ACHCS at pH < 10.

In the course of the CO_2 degassing, the supersaturation in ACHCS changes. The supersaturation degree is characterized by the ratio (the carbonate index) [4]

$$G_{37} = \frac{X_3\, X_7}{L_{37}}, \tag{3}$$

where X_3 and X_7 are the active concentrations of carbonate and calcium ions in M units, and L_{37} is the thermodynamic product of the $CaCO_3$ solubility.

The dependence of the supersaturation on the measurement number ($\Delta t = 27$ s) obtained at $t = 25\,^\circ$C is depicted in Fig. 6. A system becomes thermodynamically unstable, if $G_{37} > 1$. From Fig. 1, it follows that a reduction of the Ca^{2+} concentration starts to reveal itself, when $i > 70$. In Fig. 6, this corresponds to $G_{37} = 48$. Therefore, until $i = 70$, we have a very supersaturated state with clearly absent attributes of the crystalline $CaCO_3$ precipitation. Despite that the crystallization begins at $i > 70$, the carbonate index grows nevertheless (see Fig. 6) until $i = 88$. In other words, the generation of carbonate ions (see Figs. 2 and 5) advances their decrease due to the crystallization. During this interval, the crystalline phase precipitates on the cell surface and macroscopic-size admixtures. Micronuclei are also formed in the bulk of the parent solution. Details of the crystalline $CaCO_3$ precipitation are reflected by the variation rate of the active concentration of Ca^{2+} ions (see Fig. 7).

From Fig. 7, it follows that the rate of variation of the calcium ion concentration has some special points:

• a maximum at $i = 60$, where the growth in the activity of calcium ions is the largest as a result of the decay of ionic complexes;

• a point at $i = 70$, where the rate changes its sign, the growth of the concentration of calcium ions transforms into the decrease, and conditions for the mass precipitation of the crystalline $CaCO_3$ phase are prepared; the precipitation begins at $i > 86$ (see Figs. 1 and 3, curve *2*);

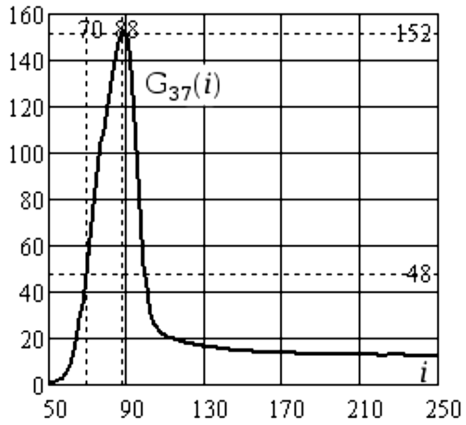

Fig. 6. Dependence of the supersaturation coefficient on the measurement number (time)

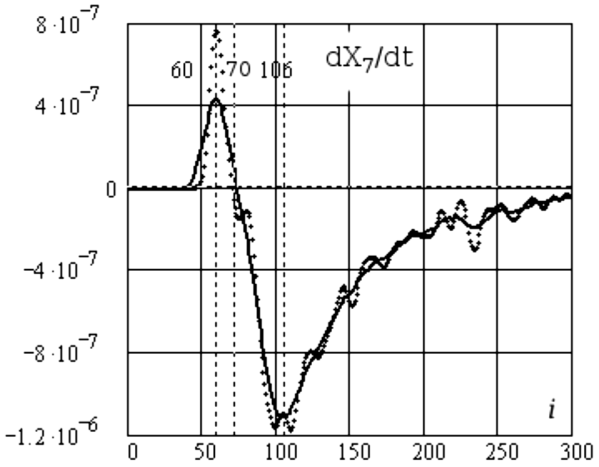

Fig. 7. Dependence of the calcium ion consumption (dX_7/dt, M/s) on the measurement number. Points correspond to initial data, and the solid curve is a result of their Gauss averaging. Vertical lines mark characteristic moments of the crystallization

• a maximum of the calcium ion decrease is at $i = 106$; at this point, the rate of precipitation of the crystalline calcium carbonate phase reaches a maximum.

The most interesting for the understanding of the process of crystalline phase precipitation is the time interval $60 < i < 85$, because it is the interval, when the crystalline phase nucleates.

Let us analyze the acceleration in the consumption of calcium ions. The acceleration curve for the variation in the concentration of calcium ions (Fig. 8) contains some more characteristic points.

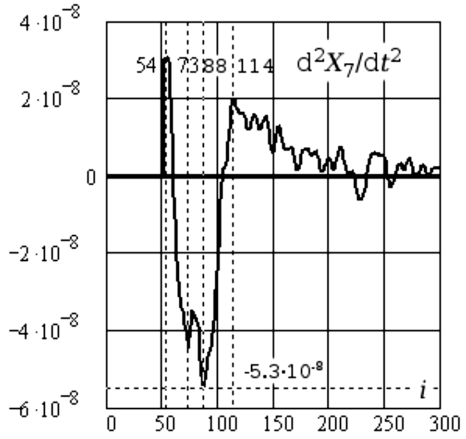

Fig. 8. Dependence of the acceleration in the calcium ion consumption (d^2X_7/dt^2) on the measurement number. Vertical lines mark characteristic points in the curve

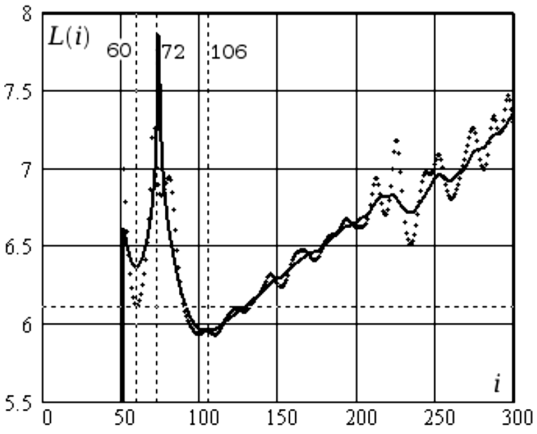

Fig. 9. Dependence of the function $L(t) = -\ln|dX_7/dt|$ on the measurement number. Points correspond to initial data, and the solid curve is a result of their Gauss averaging

• The point $i = 54$ corresponds to a maximum in the rate of growth of the active Ca^{2+} concentration obtained owing to the decay of ionic complexes (see Figs. 5–8).

• The point $i = 88$ corresponds to the maximum in the acceleration of the consumption of Ca^{2+} ions. It is of interest that this point coincides with the supersatiration maximum of G_{37} (see Fig. 6).

• The point $i = 114$ corresponds to the maximum deceleration of the rate of variation of the active Ca^{2+} concentration at the final stage of crystallization after the maximum in the consumption rate at $i = 106$ (Fig. 5).

Note that, after the point $i = 114$, both the rate and the acceleration of crystallization change monotonically. This interval begins from $G_{37}(117) = 17.6$ and practically does not terminate. ACHCS transits into a quasistationary state, which can last tens of hours. The process of $CaCO_3$ precipitation is limited at this stage by the diffusion transport of components to crystalline nuclei (see formulas (4)–(6)) and by the removal of CO_2, which becomes slower because the concentration of dissolved CO_2 approaches a value that provides an equilibrium with air.

Let us consider the precipitation kinetics for the crystalline phase of calcium carbonate. For this purpose, let us analyze the behavior of the function [10]

$$L(i) = -\ln(|\Delta X_7(t)/\Delta t|). \tag{4}$$

The dependence of this quantity on the time (the numbers of measurements) is shown in Fig. 9. This function has four pronounced characteristic sections, which were mentioned earlier:

• the first section ($50 < i < 60$) corresponds to the decay of ionic calcium complexes;

• the second section ($60 < i < 72$) corresponds to the process of crystalline phase nucleation;

• the third section ($72 < i < 106$) corresponds to the final phase of nucleation and the initial growth of crystalline nuclei, i.e. the transition between two types of kinetics (see Eqs. (8) and (9));

• the fourth section ($i > 106$) corresponds to the final phase, which is characterized by the growth of the crystalline nuclei formed earlier and is confined by the diffusion transport of the substance.

As follows from Fig. 9, during the fourth period, the time dependence of the crystallization rate logarithm can be presented by the linear function

$$\begin{aligned} &Y(i) = a + b(i - i_0), \quad a = 5.18; \\ &b = 7.18 \times 10^{-3}, \quad i_0 = 106; \end{aligned} \tag{5}$$

this yields the exponential dependence for $X_7(i)$:

$$\begin{aligned} &X_7(i) = b^{-1} \exp[-(a + b(i - i_0))] \rightarrow \\ &\rightarrow dX_7/di = -bX_7(i), \end{aligned} \tag{6}$$

where a and b are dimensionless quantities.

The comparison of Eq. (6) with experimental data results in the rate of variation of the calcium ion activity that is close to

$$dX_7/dt = -a_7[X_7(t) - X_{70}]. \tag{7}$$

In our case, $a_7 = 6.62 \times 10^{-4}$ s^{-1} and $X_{70} = 6.98 \times 10^{-4}$ M.

The dependence dX_7/dt calculated by Eq. (6) and its measured counterpart are compared in Fig. 10. One can see that the agreement between them is satisfactory at $i > 106$ (the fourth section in the variation of the rate of calcium consumption) and corresponds to the classical diffusion-driven crystallization regime. It is clear that the diffusion regime of the crystallization is inapplicable, if not the transport but the coordination and the accumulation of crystalline phase nuclei are a restricting factor, i.e. when the calcium consumption is associated with the intense nucleation and the initial growth of nuclei. As one can see from Fig. 10, the diffusion-driven crystallization regime corresponds to the interval $60 < i < 106$.

In the interval $i > 106$, the concentration of bicarbonates exceeds the concentration of carbonates by more than two orders of magnitude (see Fig. 2). Under those conditions, the most probable reaction responsible for the growth of crystalline nuclei can be the polarization deprotonization of hydrocarbonate ions in the field of a cation, e.g., a calcium ion [6, 8]:

$$\mathrm{Ca^{2+}} + \mathrm{HCO_3^-} \to \mathrm{CaCO_3} + \mathrm{H^+}. \qquad (8)$$

On the basis of Fig. 7 and curve *1* in Fig. 10, in order to simulate the active Ca^{2+} concentration kinetics, a series expansion in the coordinates of reaction (8) near the minimum point $i = 106$ was used. The result of the representation of the rate of Ca^{2+} consumption by a series is as follows:

$$dX_{71}/dt = A_{17} + B_{17}(X_1X_7 - L_{17})^2 + \\ + C_{17}(X_1X_7 - L_{17})^3, \qquad (9)$$

where, in our case (see Fig. 11), $X_1 = (\mathrm{HCO_3^-})$, $X_7 = (\mathrm{Ca^{2+}})$, $A_{17} = -1.15 \times 10^{-6}$ M/(dm^{3}s), $B_{17} = 2.53 \times 10^3$ (dm^3/M)^3/s, $C_{17} = 3.12 \times 10^7$ (dm^3/M)^5/s, $L_{17} = X_{1,i=106}X_{3,i=106} = 2.18 \times 10^{-5}$ (M/dm^3)^2. One can see that expression (9) is a good approximation for the kinetic curve describing the consumption of Ca^{2+} almost in the whole interval of observation, except for the range $i < 90$. This fact testifies that reaction (8) plays an important role at all stages of $CaCO_3$crystallization, except for the section of crystalline phase nucleation ($60 < i < 90$). Note that

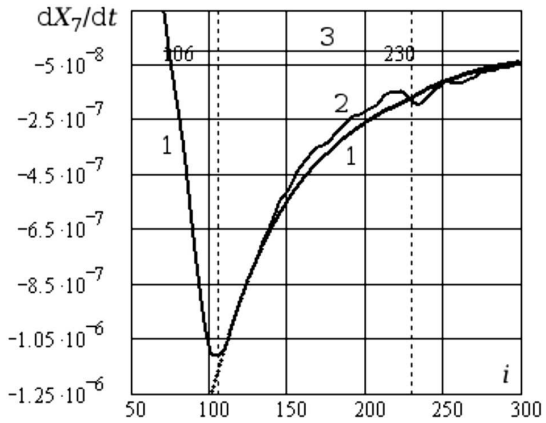

Fig. 10. Dependence of the calcium ion consumption rate (dX_7/dt, M/s) on the measurement number i: experimental data smoothed by the Gauss averaging (*1*), calculation in the framework of the diffusion model (7) (*2*), "0"-line (*3*). Vertical dashed lines mark characteristic points in the curve

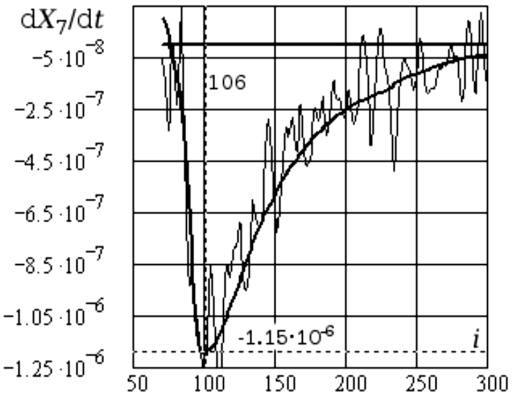

Fig. 11. Comparison of the calcium ion consumption rates (dX_7/dt, M/s). The smoothed curve was calculated by Eq. (9), the broken line exhibits raw experimental data, the horizontal lines mark the "0"-position and the minimum in the kinetic curve at $i = 106$

Eq. (9) can be used to obtain Eq. (7) as a special case, if we take into account that the Ca^{2+} concentration in our experiments was half as high as the concentration of hydrocarbonate ions. Therefore, at $i > 120$, the concentration of HCO_3^- changes weakly in comparison with that of Ca^{2+} (see Fig. 2).

The ratio between the activities X_1 and X_7 during the experiment is shown in Fig. 12. A characteristic point of the curve in Fig. 12 is a minimum at $i = 106$. It testifies to the termination of the stage of mass crystal phase nucleation, which is accompanied by the release of H^+ and CO_2 (see Figs. 3 and 4).

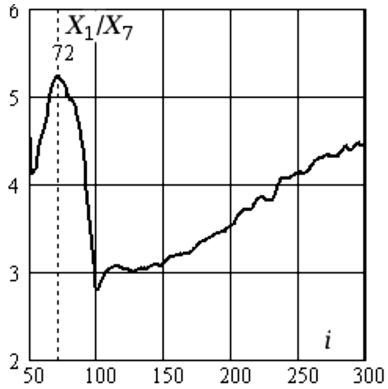

Fig. 12. Ratio between the active concentrations of hydrocarbonate and calcium ions during the experiment

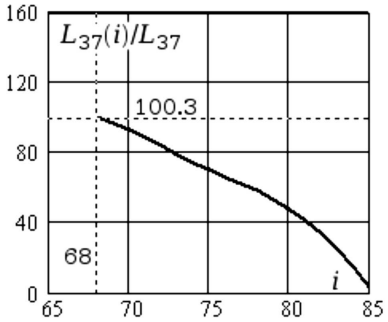

Fig. 13. Dependence of the ratio $L_{37}(i)/L_{37}$ on the measurement number i. Dashed lines mark the number of measurement, from which the ratio magnitude was analyzed

Let us analyze the initial stage of crystallization in more details. This stage corresponds to the interval $64 < i < 90$ and lasts about seven minutes until the maximum supersaturation is achieved (see Fig. 6). It is characterized by the almost constant activity of Ca^{2+} ions (see Fig. 1) and by a drastic growth of the CO_3^{2-} activity (Fig. 2, curve *2*). All that testifies that, in this case, the size of generated nuclei is so small that their total number (mol/dm^3) practically does not affect the Ca^{2+} activity. Since the nucleation (it is possible only if the product of nucleus solubility is exceeded) is a limiting process within this time interval, see Eq. (3)), we adopt that the product X_3X_7 is a reaction coordinate in this case. Despite that, let us approximate the rate of variation of the calcium ion activity in the interval $64 < i < 90$ by the expression

$$\frac{dX_7}{dt} = a_{37}[L_{37}(t) - X_3X_7], \tag{10}$$

where a_{37} is the kinetic constant. Expression (10) differs from classical ones [5, 9]: here, we used $L_{37}(t)$, the solubility product dependent on the size of crystal nuclei.

By comparing Eq. (10) with experimental data (see Figs. 7 and 11, the interval $68 < i < 90$), we obtain the coefficient $a_{37} = 1.11$ (dm^3)/(s M)$^{-1}$. Then, using Eq. (10), we calculate $L_{37}(t)$ for this interval (see Fig. 13). On the basis of experimental data on $L_{37}(i)$ and using the known relation between the size of critical nucleus $R_{\rm cr}(t)$ and $L_{37}(t)$ (see, e.g., work [13]),

$$L_{37}(t) = L_{37} \exp\left\{\frac{2\mu\sigma_{\rm cr}}{\rho_{\rm cr}R_\mu T}\frac{1}{R_{\rm cr}(t)}\right\}, \tag{11}$$

we calculate the critical equilibrium radii of crystal nuclei that are formed during the crystal nucleation. While calculating the rate of crystalline $CaCO_3$ phase formation, we also determine the concentration of crystal nuclei generated during the time t, $n(t)$. In formula (11), μ, $\rho_{\rm cr}$, and $\sigma_{\rm cr}$ are the molar mass, density, and surface energy, respectively, of crystal nuclei; R_μ the universal gas constant; T the absolute temperature; L_{37} the $CaCO_3$ solubility product. We put $\mu = 0.1$ kg/mol, $T = 298$ K; $R_\mu = 8.31$ J/(mol·K); and the unknown quantity $\sigma_{\rm ct}/\rho_{\rm cr} = 5.5 \times 10^{-3}$ J×m/kg. Under such conditions, we use Eq. (11) in order to calculate the dependences $R_{\rm cr}(t)$ and $n(t)$, which are shown in Figs. 14 and 15. From those figures, it follows that the supersaturation $G_{37} \approx 100$ ($i = 68$, corresponds to a time moment of 30 min after the experiment start), at which the crystal phase start to nucleate and which is smaller than the maximum $(G_{37})_{\max} = 152$, corresponds to crystal nuclei with $R_{\rm cr} = 8.15 \times 10^{-8}$ m.

It is of interest that, according to Fig. 14, the crystal nuclei that are formed first have almost the same size, which remains almost constant during 8 min, whereas the crystal nuclei are not visible optically owing to their small dimensions. The mass precipitation of $CaCO_3$ begins from the number $i \approx 86$ (it corresponds to a time of about 34 min from the experiment start) (see Figs. 5 and 14), when the radius of crystal nuclei reaches 3×10^{-7} m, and their concentration becomes not lower than 1.5×10^{15} m^3. This time moment corresponds to the third crystallization stage. This is the time moment (see Fig. 1), when the concentration of Ca^{2+} ions starts to decrease appreciably.

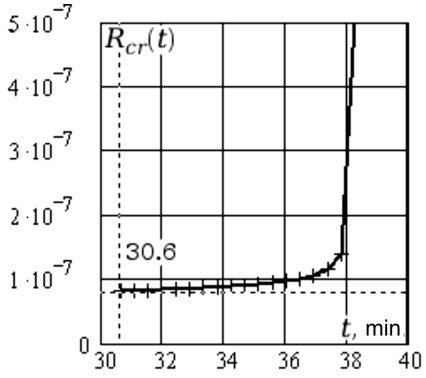

Fig. 14. Dependence of the critical radius of crystal nuclei (m) on the time (min)

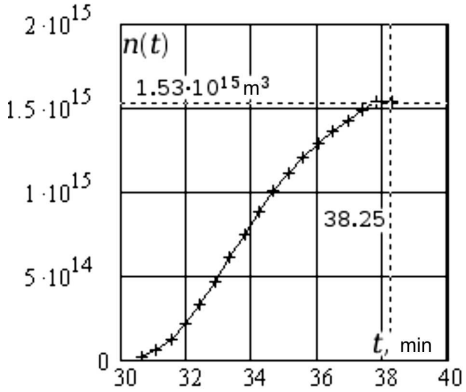

Fig. 15. Dependence of the total concentration of crystal nuclei (m^{-3}) on the time (min)

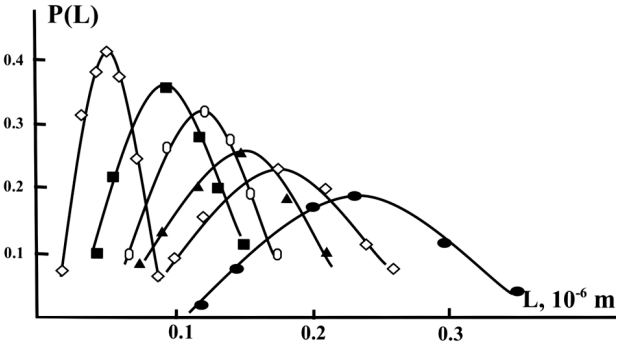

Fig. 16. Distributions of crystal nuclei over their dimensions obtained with the help of a Malver-6 counter at various times after the crystallization has begun: 20 (◇), 260 (■), 500 (0), 740 (▲), 980 (◇), and 1580 s (●)

Note that the data exhibited in Fig. 14 agree with the results of researches carried out in work [7] with the use of a Malver-6 counter (see Fig. 16, in which the dynamics of crystal nucleus distribution from the time moment of crystallization start is shown). One can see that the particles registered by a counter had an initial size of about at 5.5×10^{-8} m and were characterized by a small size dispersion.

By comparing Figs. 14 and 16, we find that, according to our estimations, the critical size of particles amounts to 8×10^{-8} m. The origin of this discrepancy may be, probably, an error made, when selecting a value of $\sigma_{\rm cr}/\rho_{\rm cr}$ for calculations or different experimental conditions. Really, in our experiments, the results of which are shown in Fig. 14, the time interval required for crystal nuclei to grow from an initial dimension to the optically observable one, i.e. from 0.08 to 0.3 μm, lasted for about 8 min (from 30 min after the experiment has begun to 38 min). At the same time, this interval equals only 20 s in Fig. 16, which is 24 times quicker. This discrepancy is connected with the fact that, in our experiments, the crystallization was initiated by a slow removal of CO_2 from the parent solution, whereas, in the experiments in Fig. 16, by a sudden mixing of components of the solution $CaCl_2$ + Na_2CO_3. However, the dimensions of crystal nuclei in our experiments and in Fig. 16 become close in the course of time.

From Figs. 14–16, one can see that, both in our experiments and in the experiments of work [7], the sets of initial crystal nuclei were almost monodisperse. This is explained by homogeneous initial conditions for the bulk crystallization. In time, the monodisperse character of nuclei in Fig. 16 becomes broken owing to the superposition of two processes: the formation and the growth of crystal nuclei. The mentioned features at the beginning of the $CaCO_3$ nucleation, in particular, the size distribution of nuclei and their growth rates that were obtained by us, agree with the later researches carried out with the help of LP-TEM technique [14].

We would like to emphasize that the almost identical results concerning the initial stages of $CaCO_3$ nucleation were obtained by us, by using inexpensive and accessible means, which are not worse by informativity than hi-tech researches such as, e.g., in works [7, 14].

4. Conclusions

1. By using an AKVA-2M complex, we managed to almost simultaneously measure the main parameters of ACHCS during the crystallization in the quasi-

continuous regime. This allowed us to study the details of the process of crystalline $CaCO_3$ precipitation from supersaturated hydrocarbonate solutions, which by their composition are close to natural surface waters, and to directly trace the major stages of crystalline $CaCO_3$ precipitation, in particular, to calculate the size and the growth kinetics of crystal nuclei.

2. During the crystal phase nucleation ($68 < i < 90$, where the CO_3^{2-} activity reaches a maximum), the activity product $(CO_3^{2-}) \cdot (Ca^{2+})$ is a reaction coordinate. At this stage, the crystallization is restricted by the coordination and the energy of interaction between ions, when the initial structure of crystalline phase is formed.

3. It is important that, for times from the interval $i > 86$ (the point, where the kinetics type changes, which corresponds to the minimum of $d^2(Ca^{2+})/dt^2$), the activity product $(HCO_3^-) \cdot (Ca^{2+})$ is a reaction coordinate. From this time moment, the curve $d(Ca^{2+})/dt$ is well approximated by an expansion series in the reaction coordinate.

4. It is shown that, at the initial stage of crystalline phase precipitation, the classical kinetic equation (10) describes the process well, if the solubility product L_{37} is taken to be dependent on the dimensions of crystal nuclei, i.e. on the energy and configuration factors [see Eq. (11)].

5. By using the time dependence of the solubility product, the critical size of crystal nuclei and their kinetics are evaluated. The former is found to equal $(7 \div 8) \times 10^{-8}$ m. This result is close to the results obtained by other researchers.

6. The time interval of the crystallization till the supersaturation maximum ($i < 86$) is characterized by the crystal phase nucleation. The dimensions of nuclei before the beginning of mass $CaCO_3$ precipitation change from 0.08 to 0.3 μm during 8 min. This time interval is the latent period of the crystal phase precipitation under the experimental conditions.

7. It is found that an almost monodisperse set of crystal nuclei with the $R_{cr} \approx 0.08$ μm is formed at the initial stage (the latent period of the crystal phase precipitation).

8. The mass precipitation of crystalline calcium carbonate is associated with the growth of already formed crystal nuclei and begins after the nuclei size exceeds 0.1 μm. This conclusion is confirmed by optical light scattering data.

9. It is shown that the diffusion mechanism of crystallization is realized at the final stage of the crystalline calcium carbonate precipitation: at $i > 106$ under our experimental conditions or, in general, after the derivative of active calcium ion concentration reaches a minimum.

10. The kinetic curves of $Ca(HCO_3)^+$, $CaCO_3^0$, and $Ca(OH)^+$ complexes are studied. It is shown that the maximum concentrations of $Ca(HCO_3)^+$ and $CaCO_3^0$ reach about 1 mM, and the concentration of $Ca(OH)^+$ is much lower than 10^{-5} mM during the experiment.

1. V.Z. Kochmarskii, V.R. Gayevskii, O.V. Kochmarskii. Prognosis of the water and hardness salt deposit compositions in circulation cooling systems. In *Proceedings of the 2nd Scientific and Engineering Conference of the Teaching Staff and Students of the UDAVG, 26 March–13 April 1996, Rivne* (UDAVG, 1996), part 3, p. 30 (in Ukrainian).
2. V.Z. Kochmars'kyi. On the mechanism of crystallization of $CaCO_3$ from water carbonate systems. *Visn. RDTU* **2**, 37 (1999) (in Ukrainian).
3. P.V. Danckwerts. *Gas-Liquid Reactions* (McGraw Hill, 1973) [ISBN: 0070097909].
4. L.S. Alekseev. The development of methods of evaluation of the stability of fresh waters. *Khim. Tekhnol. Vody* **11**, 137 (1989) (in Russian).
5. E.V. Khamskii. *Crystallization from Solutions* (Plenum Press, 1995) [ISBN: 9780306108266].
6. V.R. Gayevskii. Crystallization of $CaCO_3$ from hydrocarbonate solutions. *Visn. RDTU* **3**, 233 (2000) (in Ukrainian).
7. L.G. Vasina, A.V. Boglovskii, R.N. Calendarev. Study of the formation kinetics of calcium carbonate in a closed system.. *Trudy MEI* **466**, 53 (1980) (in Russian).
8. G.H. Nancollas, M.M. Reddy. The crystallization of calcium carbonate. II. Calcite growth mechanism. *J. Coll. Interface Sci.* **37**, 824 (1971).
9. A.M. Ivanov, V.Ya. Mikhailovskii, B.V. Galabitskii, K.A. Chervinskii. Kinetics of sodium, potassium, and calcium bicarbonate transformation in dilute aqueous solutions. *Zh. Obshch. Khim.* **49**, 481 (1979) (in Russian).
10. L.N. Plummer, D.L. Parkhurst, T.M.L. Wigley. *Chemical Modeling in Aqueous Systems*, edited by E.A. Jenne (Am. Chem. Soc., 1979) [ISBN: 9780841204799].
11. A.M. Pritchard. Deposition of hardness salts. *Fouling Sci. Technol.* **145**, 261 (1988).
12. V.Z. Kochmarskii, O.V. Kochmarskii. Anti-scale treatment of water coolant with surface-active inhibitors. *Voda Vodooch. Tekhnol.* Nos. 1–2 (43–44), 30 (2010) (in Ukrainian).
13. V.A. Kireev. *A Short Course of Physical Chemistry* (Khimiya, 1978) (in Russian).

14. L.M. Hamm, A.J. Giuffre, N. Han, J. Tao, D. Wang, J.J. Yoreo, P.M. Dove. Reconciling disparate views of template-directed nucleation through measurement of calcite nucleation kinetics and binding energies. *Proc. Natl. Acad. Sci. U.S.A.* **111**, 1304 (2014).

Received 13.09.16.
Translated from Ukrainian by O.I. Voitenko

В.З. Кочмарський, В.Р. Гаєвський, Н.Л. Тишко

КРИСТАЛІЗАЦІЯ КАРБОНАТУ
КАЛЬЦІЮ З ГІДРОКАРБОНАТНИХ РОЗЧИНІВ

Р е з ю м е

Досліджувалася кінетика виділення $CaCO_3$ з модельних розчинів, утворених попереднім насиченням деіонізованої води CO_2 з додаванням $NaHCO_3$ та $CaCl_2$. Особливістю методики є практично одночасне вимірювання активностей основних компонент кальцій-гідрокарбонатної водної системи (КГКВС): Ca^{2+}, CO_2, CO_3^{2-}, pH і температури. Кристалізація $CaCO_3$ забезпечувалася дегазацією CO_2 повітрям. Впродовж дегазації процеси в КГКВС поділяються на чотири стадії: розпад кальцієвих комплексів; утворення зародків твердої фази (ЗТФ) в об'ємі розчину; перехідна стадія – заключна фаза утворення ЗТФ та початок їх росту; масове виділення $CaCO_3$, що відповідає інтенсивному росту ЗТФ. Для другої стадії кристалізації координатою реакції є добуток $(Ca^{2+}) \cdot (CO_3^{2-})$, а для третьої та четвертої – $(Ca^{2+}) \cdot (HCO_3^-)$. Для другої стадії, використовуючи поняття добутку розчинності $CaCO_3$, залежного від розмірів ЗТФ, розраховано розміри та кінетика росту ЗТФ і їх концентрація. Впродовж процесу утворення ЗТФ їх розмір практично сталий ($\approx 8 \cdot 10^{-8}$ м), а концентрація сягає $1{,}5 \cdot 10^{15}$ м$^{-3}$. Масове виділення $CaCO_3$ (четверта стадія) починається при досягненні ЗТФ розміру $\approx 3 \cdot 10^{-7}$ м.